



HAL
open science

Influence of oil saturation upon spectral induced polarization of oil-bearing sands

M. Schmutz, A. Revil, P. Vaudelet, M. Batzle, P. Femenía Viñao, D. D. Werkema

► **To cite this version:**

M. Schmutz, A. Revil, P. Vaudelet, M. Batzle, P. Femenía Viñao, et al.. Influence of oil saturation upon spectral induced polarization of oil-bearing sands. *Geophysical Journal International*, 2010, 183, pp.211-224. 10.1111/J.1365-246X.2010.04751.X . insu-00565038

HAL Id: insu-00565038

<https://insu.hal.science/insu-00565038>

Submitted on 10 Mar 2021

HAL is a multi-disciplinary open access archive for the deposit and dissemination of scientific research documents, whether they are published or not. The documents may come from teaching and research institutions in France or abroad, or from public or private research centers.

L'archive ouverte pluridisciplinaire **HAL**, est destinée au dépôt et à la diffusion de documents scientifiques de niveau recherche, publiés ou non, émanant des établissements d'enseignement et de recherche français ou étrangers, des laboratoires publics ou privés.

Influence of oil saturation upon spectral induced polarization of oil-bearing sands

M. Schmutz,¹ A. Revil,^{2,3} P. Vaudelet,¹ M. Batzle,² P. Femenía Viñao² and D. D. Werkema⁴

¹Institut EGID, Université Bordeaux 3, 33607 Pessac, France

²Colorado School of Mines, Department of Geophysics, Golden, CO, USA

³INSU-CNRS LGIT UMR 5559, Université de Savoie, Equipe Volcans, Le Bourget du Lac, France. E-mail: arevil@mines.edu

⁴U.S. EPA, ORD, NERL, ESD, CMB, Las Vegas, NV, USA

Accepted 2010 July 25. Received 2010 June 26; in original form 2010 March 13

SUMMARY

The induced polarization model developed recently by Revil and Florsch to understand the complex conductivity of fully saturated granular materials has been extended to partial saturation conditions. It is an improvement over previous models like the Vinegar and Waxman model, which do not account explicitly for the effect of frequency. The Vinegar and Waxman model can be considered as a limiting case of the Revil and Florsch model in the limit where the distribution of relaxation times is very broad. The extended model is applied to the case of unconsolidated sands partially saturated with oil and water. Laboratory experiments were performed to investigate the influence of oil saturation, frequency, grain size, and conductivity of the pore water upon the complex resistivity response of oil-bearing sands. The low-frequency polarization (below 100 Hz) is dominated by the polarization of the Stern layer (the inner part of the electrical double layer coating the surface of the grains in contact with water). The phase exhibits a well-defined relaxation peak with a peak frequency that is dependent on the mean grain diameter as predicted by the model. Both the resistivity and the magnitude of the phase increase with the relative saturation of the oil. The imaginary (quadrature) component of the complex conductivity is observed to decrease with the oil saturation. All these observations are reproduced by the new model.

Key words: Electrical properties; Electromagnetic theory; Hydrogeophysics; Permeability and porosity.

1 INTRODUCTION

Induced polarization represents the measurement of the conductivity response (magnitude and phase) over a frequency range typically occurring from 1 mHz (sometimes down to the microhertz, see Olhoeft 1985) to a few tens of kilohertz. Two electrodes are used to inject and retrieve the electrical current and two electrodes are used to measure the resulting difference of electrical potential and the phase lag between the current and the voltage (Marshall & Madden 1959; Olhoeft 1986; Sturrock 1999; Lesmes & Morgan 2001; and Slater & Lesmes 2002a). In addition to the classical applications of induced polarization to the prospection of ore bodies, this non-intrusive method has been used for environmental purposes, especially to investigate contaminant plumes (Olhoeft 1986; Slater & Lesmes 2002b) and to interpret down-hole measurements in oil-bearing sediments (Vinegar & Waxman 1982, 1984).

In this study, we are interested in the effect of a non-wetting (NW) oil in the pore space of a porous sand upon the measurements of the spectral induced polarization. The presence of oil in porous

materials has a characteristic electrical signature that depends on the amount of polar components in the oil and therefore depends on its wettability with respect to the solid phase (Olhoeft 1986; Börner *et al.* 1993). Therefore the electrical signature of an oil-bearing sand also depends on the maturity of the oil or the time in which the oil has existed in the subsurface. This time dimension is one of the main factors controlling the biodegradation and the biogeophysical response of oil spills. Previous works have already shown that the induced polarization response of unsaturated porous materials changes with the saturation of the water phase (Vinegar & Waxman 1982, 1984; Ulrich & Slater 2004; Binley *et al.* 2005; Ghorbani *et al.* 2008). Olhoeft (1986) reported an increase of the phase of materials containing clay particles and contaminated with oil. Vanhala *et al.* (1992) described the spectral induced polarization signature associated with the presence of toluene, heptane, and ethylene glycol in glacial tills. They observed an increase of the magnitude of the phase in the presence of these organic contaminants. Börner *et al.* (1993) observed an increase of the magnitude of the phase in clays in the presence of organic contaminants and a decrease of the magnitude of the phase for oil contaminated

sandstones except in the case of benzene. Vanhala (1997) showed that the introduction of motor oil decreases the magnitude of the phase of glacial sediments (sands and tills). Recently, Cassiani *et al.* (2009) performed an investigation showing the effect of the saturation in hydrocarbons upon induced polarization (using a NW oil) but they investigated only few extreme values in the oil saturation. They were able to fit their data with the empirical Cole–Cole model but this empirical relationship does not explain the experimental results from a mechanistic standpoint.

With the exception of the work of Vinegar & Waxman (1984), no quantitative model has been developed to interpret the available experimental data and to see what fundamental mechanisms could explain these experimental observations. Vinegar & Waxman (1984) were the first to develop a model based on the polarization of the Stern layer plus the effect of membrane polarization. However, they did not account for frequency dependence of the in-phase and quadrature conductivities and therefore were not able to explain experimental data showing peaks in the phase lag or quadrature conductivity.

In this investigation, we performed new laboratory experiments showing the influence of oil saturation, grain size, and conductivity of the pore water upon the complex resistivity response of oil-bearing sands. In addition, we developed a quantitative and testable model to explain these experimental results. This model is based on a description of the polarization of the electrical double layer at the grain/water interface and is an extension of the model published recently by Revil & Florsch (2010).

2 THEORETICAL BACKGROUND

There exist numerous models describing the high-frequency electromagnetic properties of partially saturated sedimentary rocks. However, to the best of our knowledge, the only quantitative model proposed in the literature to account for the effect of oil saturation upon low-frequency (<100 Hz) complex conductivity measurements of partially saturated sandstones is the model developed by Vinegar & Waxman (1982, 1984). A description of this model is provided in Appendix A. However, this model does not account for the frequency dependence of the in-phase and quadrature conductivities and therefore needs to be extended with that respect. We will show that the Vinegar & Waxman (1982, 1984) model could be considered as the limiting case of a model accounting explicitly for the grain size distribution.

Recently a new model has been developed by Revil & Florsch (2010) in terms of providing a linear quantitative model for the low-frequency complex conductivity of a partially saturated pack of sand grains. The grain size distribution is characterized by a median D_{50} and a standard deviation $\hat{\sigma}$. This model was developed to relate quantitatively spectral induced polarization to permeability for fully water-saturated granular media. It accounts explicitly for the grain size distribution through a polarization of the electrical double layer coating the surface of the grains. At low frequencies (typically below 100 Hz), the main induced polarization mechanism discussed by Revil & Florsch (2010) corresponds to the polarization of the inner portion of the electrical double layer, the so-called Stern layer (Fig. 1). The external part of the electrical

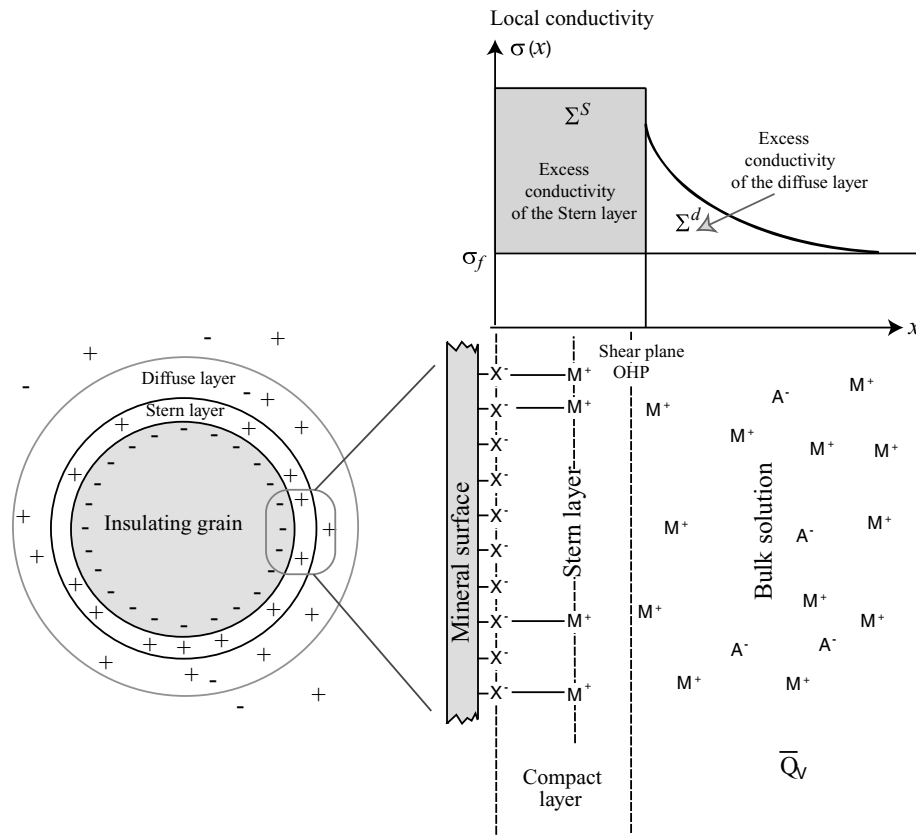


Figure 1. Sketch of the electrical double layer at the pore water interface for a fully water-saturated sand. The electrical double layer is made of the Stern layer with mobile counterions able to move tangentially along the mineral surface and the diffuse layer of counterions and coions existing in the vicinity of the mineral/water interface. For a pack of silica grains, the main polarization mechanism seems to be associated with the polarization of the Stern layer. The conductivities Σ^S and Σ^d are the specific surface conductivities (in S) of the Stern and diffuse layers, respectively, and \bar{Q}_V is the excess of charge of the pore water per unit pore volume at full water saturation and due only to the contribution of the diffuse layer coating the surface of the pores.

double layer only contributes to the DC conductivity and is considered to be independent of the frequency. An additional mechanism, called Maxwell–Wagner polarization, is also known to contribute at higher frequencies. Although the electrical double layer polarization is due to the accumulation of charge carriers at some discontinuities in the porous material (implying the existence of polarization length scales), the Maxwell–Wagner polarization is due to the discontinuity of the current displacement at the interface between the different phases of the porous material. The Maxwell–Wagner contribution is therefore dielectric in nature. This dielectric contribution can be dominant above 1 kHz (e.g. Lesmes & Morgan 2001; Leroy *et al.* 2008). In this paper, we are mainly interested in the low-frequency content of the induced polarization spectra for which the Stern layer polarization seems to dominate, so we ignore the Maxwell–Wagner polarization effect and we consider only our data in the frequency range 1 mHz–100 Hz because the effect of the saturation upon the Maxwell–Wagner polarization is fairly well-known.

In a water-saturated sand, the polarization of the Stern layer occurs because the Stern layer is discontinuous at the scale of the representative elementary volume. Indeed, the grains are in contact with each other but the grain-to-grain contiguity provides only a continuous pathway for the diffuse layer that extends few nanometers to tens of nanometers in the pore space. The Stern layer formed by the sorption of counterions (generally cations) on the mineral surface remains discontinuous at the grain-to-grain contacts. In addition, we consider that sorption–desorption processes of the counterions do not appear in the investigated frequency range (1 mHz–100 Hz). Therefore, when an electrical field is applied to a grain, the electromigration of the weakly sorbed cations of the Stern layer (moving in the direction of the electrical field) accumulate at the edge of the grain and back-diffuse in their concentration gradients (Leroy *et al.* 2008, Revil & Florsch 2010). This idea is not new and is essentially the same as proposed by Schwarz nearly 50 years ago (Schwarz 1962). Schwarz studied the polarization of a compact layer of counterions coating the surface of an insulating sphere. He based his approach on the assumption that there is no exchange of ions between the Stern and the diffuse layers or the pore water. He therefore assumed that the counterions can only move tangentially along the surface of the grains. This assumption seems plausible as the kinetics of sorption/desorption of ions in the Stern layer is very slow (typically several hours, see discussion in Revil *et al.* 1999, their fig. 7 and Li *et al.* 2010). We consider therefore that the characteristic length scale associated with this polarization mechanism is related to the size of the grains. In the model developed by Revil & Florsch (2010), the influence of a grain size distribution is accounted for through the use of a convolution product (see also Lesmes & Morgan 2001).

In the presence of a partially saturated oil sand with a NW oil, the pore volume is filled by two continuous and immiscible fluid phases, a wetting fluid and a NW fluid. In this investigation, the wetting fluid is water (subscript w) and the NW fluid is oil (subscript o). We denote $s_w \in [0; 1]$ the relative saturation of the water phase and $s_o = 1 - s_w$ is therefore the oil relative saturation. A sketch of the distribution of the different phases in the presence of a NW oil is shown in Fig. 2(a). When oil is the NW phase, the diffuse layer coating the surface of the sand grains is supposed to stay continuous over a representative elementary volume of the sand including at high oil saturation because oil is the NW phase. The situation would be very different for a wetting oil as the electrical response would be possibly controlled by the properties of the electrical double

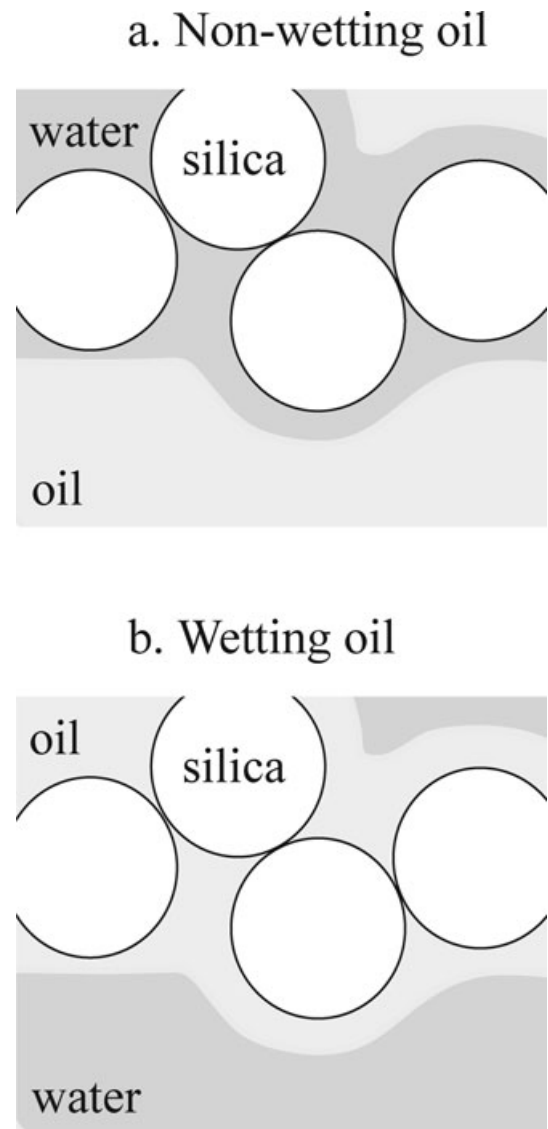


Figure 2. Sketch showing the difference in the position of the different phases between the solid phase, oil, and the pore water depending on the wettability of the oil with respect to the solid phase (silica). (a) Oil is the NW fluid. They are two interfaces that may carry an electrical double layer: the solid/water interface and the oil/water interface. The electrical diffuse layer of the pore water is squeezed in a smaller volume when the saturation of the oil phase increases. (b) Oil is the wetting phase.

layer at the oil/water interface rather than by the properties of the solid/water interface (see Fig. 2).

We denote $\omega = 2\pi f$ the angular frequency, f the frequency (in Hz), and $i = (-1)^{1/2}$ the pure imaginary number. The magnitude of the conductivity $|\sigma|$ and the phase lag φ are related to the real (in-phase) and imaginary (out-of-phase or quadrature) components of the complex conductivity σ^* , σ' and σ'' (expressed in S m^{-1}) by

$$\sigma^* = |\sigma| \exp(i\varphi) = \sigma' + i\sigma'', \quad (1)$$

$$|\sigma| = \sqrt{\sigma'^2 + \sigma''^2}, \quad (2)$$

$$\tan \varphi = \frac{\sigma''}{\sigma'}. \quad (3)$$

Induced polarization is usually displayed as a resistivity magnitude $|\rho| = 1/|\sigma|$ (in ohm m) and a phase φ (in rad) or alternatively as in-phase and quadrature conductivities, σ' and σ'' , respectively. We will use both representations later because the quadrature conductivity is directly related to surface conductivity whereas the phase angle depends on both the in-phase and quadrature conductivities.

In this paper, we do not account (1) for the Maxwell–Wagner polarization occurring at higher frequencies (>100 Hz) and (2) the conductivity of the oil, which is assumed to be insulating like the silica grains. As explained previously, the Stern layer is discontinuous at the scale of the grains and therefore the relevant polarization length scale is the grain size. The diffuse layer is continuous because it extends inside the pore space and therefore surrounds continuously all the grains. The oil phase is assumed to be continuous and the oil–water interface is assumed to be uncharged. Using the approach of Revil & Florsch (2010) (see also Leroy *et al.* 2008 and Leroy & Revil 2009), the low-frequency complex electrical conductivity is written as (see Appendix B),

$$\sigma(\omega) = \frac{s_w^n}{F} \left[\sigma_w + \beta_{(+)} \frac{\bar{Q}_V}{s_w} + (F-1) \frac{\sigma_S(\omega)}{s_w} \right], \quad (4)$$

where

$$\sigma_S(\omega) = 4E_h \Sigma^S \left(1 - \int_0^\infty \frac{g(\tau)}{1 + i\omega\tau} d\tau \right), \quad (5)$$

$$E_h = \int_0^{+\infty} f(D) d \ln D, \quad (6)$$

$$\int_0^\infty g(\tau) d\tau = 1, \quad (7)$$

and $F = \phi^{-m}$ is the electrical formation factor (m is called the cementation exponent and ϕ is the connected porosity), n is the saturation exponent (also called the second Archie's exponent, Archie 1942), the term $\beta_{(+)} \bar{Q}_V$ (in S m^{-1}) represents the surface conductivity associated with the excess of charges in the pore water (the so-called diffuse layer contribution, see Revil *et al.* 2005), \bar{Q}_V (in C m^{-3}) is the excess of charge per unit pore water volume due to the diffuse layer, $\beta_{(+)}$ (in $\text{m}^2 \text{s}^{-1} \text{V}^{-1}$) represents the mobility of the cations in the main pore space assumed to be the same in the bulk pore water and in the Stern layer, σ_w is the conductivity of the pore water, σ_S is the equivalent conductivity of the grains coated by the Stern layer (in S m^{-1}), $g(\tau)$ represents the probability distribution of the relaxation times τ , E_h (in m^{-1}) is the expected value of the probability density function $h(\eta)$, which is the probability density distribution of the inverse of the grain diameter $\eta = 1/D$ (D is the grain diameter) and $f(D)$ is the probability density of the grain diameter distribution (see Revil & Florsch 2010 for details). The assumption that the mobility is the same in the bulk pore water and in the Stern layer should be considered with caution: This assumption may be valid for counterions that are weakly sorbed in the Stern layer (like sodium that keeps its hydration shell in the Stern layer) but obviously does not hold for counterions that are strongly sorbed on the mineral surface. A discussion on this subject is provided in Revil & Florsch (2010).

The saturation dependence of eq. (4) is consistent with the model and experimental data of Vinegar & Waxman (1982, 1984) (see Appendix A for a check of the consistency between the two models). However, the model of Vinegar & Waxman (1982, 1984) does not explicitly account for the frequency dependence of the in-phase and quadrature conductivities and the influence of the grain size

distribution whereas our model accounts explicitly for these dependencies. The reason for this discrepancy is the following: Vinegar & Waxman (1982, 1984) worked with rocks characterized by a very broad distribution of heterogeneities that translate into a very broad distribution of relaxation times. Therefore, the convolutive effect of the heterogeneity is responsible for the lack of dependence of the in-phase and quadrature components of the conductivity with the frequency over a quite broad frequency range. In our case, the distribution of the heterogeneities is mainly controlled by a narrow grain size distribution and we will clearly see the peak in the phase associated with the expected value of this distribution. As explained in Appendix A, our model can be considered as an extension of the Vinegar & Waxman model accounting explicitly for the effect of the frequency.

The so-called surface conductivity $\bar{\sigma}_S(\omega) = \sigma'_S(\omega) + i\sigma''_S(\omega)$ associated with the Stern layer shown in Fig. 1 can be decomposed into a real component and a quadrature component,

$$\sigma'_S(\omega) = \sigma_S^\infty \left(1 - \int_0^\infty \frac{g(\tau)}{1 + \omega^2\tau^2} d\tau \right), \quad (8)$$

$$\sigma''_S(\omega) = \sigma_S^\infty \int_0^\infty \frac{\omega\tau}{1 + \omega^2\tau^2} d\tau, \quad (9)$$

$$\sigma_S^\infty = 4\Sigma^S E_h. \quad (10)$$

The grain size distribution of the sand that we will consider later in this paper is log normal,

$$f(D) = \frac{1}{\sqrt{2\pi}\hat{\sigma}} \exp \left[-\frac{(\ln D - \mu)^2}{2\hat{\sigma}^2} \right], \quad (11)$$

with $\hat{\sigma} = \ln \sigma_g$ and $\mu = \ln D_{50}$ are the standard deviation and the mean of the grain diameter natural logarithm, respectively, σ_g is the geometric standard deviation, and D_{50} represents the median of the grain size distribution. The median D_{50} (in m) is used as a measure of the average particle diameter size for the granular material. The standard deviation is a measure of the dispersion about the mean grain diameter for a given distribution. In this case, the expectation of the distribution of the inverse of the grain size is given by

$$E_h = \exp \left(\frac{1}{2} \hat{\sigma}^2 - \mu \right) = \frac{1}{D_{50}} \exp \left(\frac{1}{2} \hat{\sigma}^2 \right). \quad (12)$$

For such a grain size distribution, the related distribution of the relaxation times is given by Revil & Florsch (2010)

$$g(\tau) = \frac{1}{\sqrt{2\pi}(2\hat{\sigma})\tau} \exp \left[-\left(\frac{\ln(\tau/\tau_0)}{\sqrt{2}(2\hat{\sigma})} \right)^2 \right]. \quad (13)$$

Note that the standard deviation for the distribution of the relaxation times is $2\hat{\sigma}$ and not $\hat{\sigma}$. In the model developed by Schwarz (1962), the relaxation time for an ion of species i , τ_0 (in s), is therefore related to the diffusion coefficient of the ion i in the Stern layer D_S^i by

$$\tau_0 = \frac{\alpha D_{50}^2}{8D_S^i}. \quad (14)$$

where $\alpha = F\phi$ is the tortuosity given by the product of the formation factor F with the connected porosity ϕ . This tortuosity correction does not appear in the original paper of Schwarz (1962) and is due to Binley *et al.* (2010). For the sands investigated in this paper, the formation factor is 3.9 and the porosity is 0.4. This yields a bulk tortuosity equal to 1.56.

On a silica surface, surface conductivity is generally very small with respect to the pore water conductivity (except for very fresh pore waters). We assume conditions such as the conductivity term associated with the pore water is larger than the surface conductivity term $(F - 1)\sigma_S^\infty$. This condition is satisfied for the tap water and is a quite good approximation for the demineralized water used below in the experiments. Neglecting the contribution of the surface conductivity to the in-phase conductivity and assuming that the grain size distribution is described by the delta function, the in-phase and quadrature conductivities and the phase are given by

$$\sigma' \approx \frac{s_w^n}{F} \sigma_w, \quad (15)$$

$$\sigma'' = -\frac{s_w^n}{F} \sigma_S^\infty (F - 1) \frac{\omega \tau_0}{1 + \omega^2 \tau_0^2}, \quad (16)$$

$$\varphi = \text{atan} \left[\frac{-\sigma_S^\infty (F - 1) \frac{\omega \tau_0}{1 + \omega^2 \tau_0^2}}{s_w \sigma_w + (F - 1) \sigma_S^\infty \left(1 - \frac{1}{1 + \omega^2 \tau_0^2}\right)} \right], \quad (17)$$

$$\varphi \approx -\text{atan} \left[\frac{\sigma_S^\infty (F - 1) \omega \tau_0}{s_w \sigma_w (1 + \omega^2 \tau_0^2)} \right], \quad (18)$$

respectively.

In our model, we do not consider polarization for the diffuse layer because we assume that it forms a continuous phase through the porous material even at low pore water saturations as long as oil is the NW phase. In contrast, the Stern layer polarizes because it is discontinuous. However the assumption that the polarization is entirely due to the Stern layer should be consider with caution as other contributions, such as the membrane polarization, have not been considered yet from a quantitative standpoint (see a short discussion in Leroy & Revil 2009).

An alternative view of the problem is to consider the influence of the specific surface area, S , upon the phase or the quadrature conductivities. It is generally admitted that the higher the specific surface area, the higher the polarization and therefore the quadrature conductivity. The surface area per pore volume ratio is related to the expectation E_h by

$$\frac{S}{V_p} \approx \frac{6}{\phi} \frac{1}{E_h}, \quad (19)$$

$$\frac{S}{V_p} \approx \frac{6}{D_{50} \phi} \exp\left(\frac{1}{2} \hat{\sigma}^2\right), \quad (20)$$

where ϕ represents the connected porosity. Therefore the mean grain size, the standard deviation of the grain size distribution, the connected porosity, and the surface to pore volume ratio are all connected parameters through eq. (19) or eq. (20).

We note φ_0 the value of the phase at the relaxation frequency (in s^{-1}) defined by $\omega_0 = 1/\tau_0$, where τ_0 is given by eq. (14). Note that the relaxation occurs at a frequency that is, in principle, independent on the saturation of the water phase. As successfully explained by Jougnot *et al.* (2010) for clay-rocks (argillites), the effect of the saturation upon the phase is due to the fact that the Maxwell–Wagner is not entirely negligible at the frequency at which the relaxation of the Stern layer occurs. An alternative possibility would be that there is a small contribution from membrane polarization that is saturation-dependent because occurring in the pore water phase

and not along the mineral surface. Using eq. (18), this phase is given by

$$\varphi_0 \approx -\frac{(F - 1)\sigma_S^\infty}{2s_w \sigma_w + (F - 1)\sigma_S^\infty}. \quad (21)$$

Our model predicts therefore a change of the phase peak with the saturation. Using this high salinity assumption, we obtain

$$\varphi_0 \approx -\frac{\sigma_S^\infty (F - 1)}{2s_w \sigma_w}. \quad (22)$$

Using eqs (8) and (12) with the grain size distribution assumed to be described by a log normal distribution, the high frequency surface conductivity is given by

$$\sigma_S^\infty = \frac{2}{D_{50}} \Sigma^S \exp\left(\frac{1}{2} \hat{\sigma}^2\right), \quad (23)$$

and therefore the phase peak is given by

$$\varphi_0 \approx -\frac{2\Sigma^S (F - 1)}{\sigma_w D_{50}} \exp\left(\frac{1}{2} \hat{\sigma}^2\right) s_w^{-1}. \quad (24)$$

Neglecting the surface conductivity in the in-phase conductivity (for the brine saturated case), the in-phase and quadrature conductivities at the phase peak are given by

$$\sigma'_0 \approx \frac{s_w^n}{F} \sigma_w, \quad (25)$$

$$\sigma''_0 = -\frac{s_w^{n-1}}{2F} \sigma_S^\infty (F - 1). \quad (26)$$

Replacing the surface conductivity σ_S^∞ by its expression as a function of the specific surface conductance, see eq. (23), the quadrature conductivity at the relaxation frequency can be written as

$$\sigma''_0 = -\frac{1}{D_{50}} \left(\frac{F - 1}{F}\right) \Sigma^S \exp\left(\frac{1}{2} \hat{\sigma}^2\right) s_w^{n-1}. \quad (27)$$

The sign “-” in this equation means that the phase lag between the current and the voltage is negative (if the current is imposed, the voltage follows the current with a phase lag). These equations will be tested later in Section 4.

A last point that is worth of discussion is the influence of the oil water interface upon complex conductivity. In Fig. 2, two end-members cases correspond to the cases of a pure NW oil and a pure wetting oil. In the first case, there are two interfaces to consider in principle in the pore space: the grain/water interface and the oil/water interface. The model discussed earlier does consider only the grain/water interface. This assumption is valid if the oil/water interface is non-reactive and therefore does not form an electrical double layer in water or if the specific surface area of the oil/water interface is much smaller than the specific surface area of the grain/water interface. Experimental data shows however that there is an electrical double layer at the oil/water interface including for NW oils (Volkov *et al.* 1996). However, if the oil phase form a continuous phase in the pore space of the porous material, we should not expect any polarization of the Stern layer of the oil/water interface.

The case of a wetting oil should be quite different. Indeed, in the extreme case where oil covers uniformly the surface of the grains, there is only one interface (the oil/water interface) and the polar components contained in the oil (e.g. asphaltenes) makes the oil/water interface quite reactive in water and the setting of a strong electrical double layer. However this second case in not investigated in this paper and will be investigated in a separate contribution.

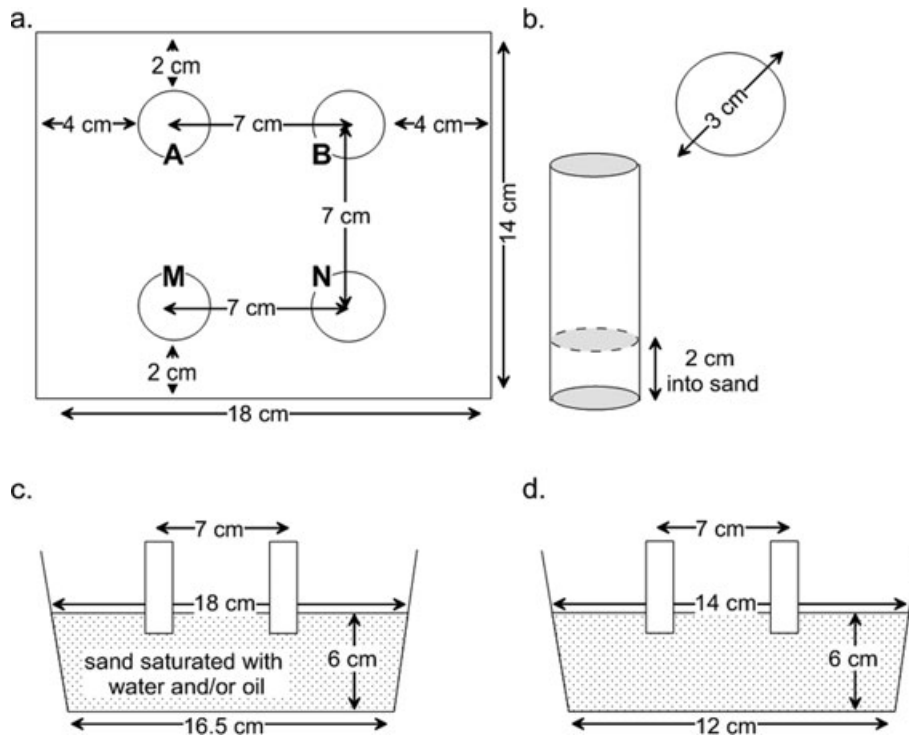


Figure 3. Sketch of the experimental setup using the Petiau Pb/PbCl₂ electrodes manufactured by Geonesis. (a) View of earlier. (b) Size of the Petiau electrodes (from Geonesis). (c and d) Views from the side.

3 MATERIAL AND METHODS

As explained in Section 2, the spectral induced polarization method is based on the measurements of the complex resistivity ρ^* (in ohm m) over several decades in frequency (in this case from 1 mHz to 45 kHz). The complex resistivity is the inverse of the complex conductivity σ^* : $\rho^* = 1/\sigma^*$. What is actually measured is the complex resistance or impedance R^* (in ohm) between the end-faces of a cylindrical sample for instance:

$$R^*(\omega) = \frac{U}{I} = |R^*(\omega)| e^{i\varphi(\omega)}, \quad (28)$$

where U is the measured voltage difference between electrodes M and N, which are called the potential electrodes (see Fig. 3), I the magnitude of the imposed current between the electrodes A and B, which are called the current electrodes (Fig. 3), and $|R^*(\omega)|$ and $\varphi(\omega)$ are the amplitude and the phase of the complex impedance, respectively. The complex resistivity ρ^* is related to R^* by a geometrical factor K (in m): $\rho^*(\omega) = K R^*(\omega)$. This geometrical factor K takes into account not only the position of the electrodes in the tank but also the insulating boundary conditions at all boundaries (Fig. 3). The insulating boundary condition means that the normal component of the current density and the electrical field are equal to zero at the boundaries. The geometrical factor was calibrated by measuring the conductivity of the sand independently with a two-electrode device and a cylindrical cell at 4 kHz (at this frequency, the polarization of the stainless steel electrodes can be neglected). Note that the phase $\varphi(\omega)$ is the same for the resistivity and the impedance and is independent on the value of the geometrical factor K .

To perform the experiments, we used a small tank filled with a mix of oil, water and sand grains (Fig. 3). The amount of sand was kept the same and only the volumetric proportion of oil and water was changed. A sketch of the experimental setup is shown in Fig. 3. Both demineralized and tap waters were used. The conductivity of the tap

Table 1. Measured properties of the loosely compacted sands used in this study (from Sakaki & Illangasekare 2007 and Sakaki 2009). These measurements include the connected porosity ϕ , the hydraulic conductivity at saturation K_s , the mean grain diameter D_{50} , and the standard deviation of the log normal grain size distribution $\hat{\sigma}$.

Sand type	ϕ (-)	K_s (10^{-3} m s^{-1})	D_{50} (mm)	$\hat{\sigma}$
Type B(#30)	0.42	1.16 ± 0.09	0.5	0.2
Type A(#70)	0.42	0.141 ± 0.15	0.2	0.3

water was comprised between $1.20 \times 10^{-2} \text{ S m}^{-1}$ and $1.70 \times 10^{-2} \text{ S m}^{-1}$ at 25°C. The electrical conductivity of the demineralized water was $5 \times 10^{-4} \text{ S m}^{-1}$ at 25°C. The sand was a silica sand with the properties summarized in Table 1. The properties of this sand were measured by Sakaki & Illangasekare (2007), and Sakaki (2009). We used two sands denoted as Types A and B, respectively. Type A has a mean grain diameter of 200 μm whereas Type B has a mean grain diameter of 500 μm .

All the experiments have been done under the same conditions, at ambient laboratory temperatures, typically $24 \pm 3^\circ\text{C}$ using exactly the same procedure. The composition of the tap water is given in Table 2 (mass density 1000 kg m^{-3}). The light North Sea oil has a mass density of 898 kg m^{-3} . Its composition is reported in Table 3. So the difference in mass density between water and oil is quite small. The plastic tank used for the experiments has a height of 8 cm, a length of 15 cm, and a width of 10 cm.

The spectral induced polarization measurements were conducted using a ZEL-SIP04 impedance-meter developed at the Forschungszentrum, Juelich, Germany by Egon Zimmermann. The characteristics of this apparatus including its accuracy and reliability were described extensively by Zimmermann *et al.* (2008) and are not repeated here. An additional test can be found in Jougnot *et al.* (2010). The sensitivity of this apparatus is typically at 0.1 mrad

Table 2. Composition of the tap water (from City of Golden 2009) with the assumption that hardness is due to calcium. This yields a TDS of 245 ppm ($\sim 4.9 \times 10^{-2} \text{ S m}^{-1}$ at 25°C). Measurement made in April–May 2009.

Substance	Concentration (mmol/l)
Ca ²⁺	0.95
K ⁺	0.09
Na ⁺	1.44
Cl ⁻	1.30
SO ₄ ²⁻	0.82
HCO ₃ ⁻	0.75
pH	8.4

Table 3. Composition of the oil (in weight per cent) used for the experiments.

Molecules	Weight fraction (per cent)
Butanes	0.0
Pentanes	0.0
Hexanes	0.0
Heptanes	0.3
Octanes	0.5
Nonanes	1.0
Decanes	1.4
Undecanes	1.9
Dodecanes	2.5
Tridecanes	3.1
Tetradecanes	3.7
Pentadecanes	4.1
Hexadecanes	3.7
Heptadecanes	3.8
Octadecanes	4.0
Nonadecanes	3.8
Eicosanes	3.8
Heneicosanes	3.3
Docosanes	3.0
Tricosanes	2.8
Tetracosanes	2.7
Pentacosanes	2.5
Hexacosanes	2.3
Heptacosanes	2.4
Octacosanes	2.2
Nonacosanes	2.2
Triacosanes	2.2
Untriacontanes	2.2
Dotriacontanes	1.8
Tritriacontanes	1.7
Tetracontanes	1.5
Pentatriacontanes	1.7
Hexatriacontanes	1.4
Heptatriacontanes	1.1
Octatriacontanes	1.0
Nonatriacontanes	1.0
Tetracontanes	1.0
C40+	22.5
Total	100.0

over most of the investigated spectrum. A test reported in Jougnot *et al.* (2009) using a pure carbonate rock sample show no phase as expected for this type of material.

At a room temperature of $24 \pm 3^\circ\text{C}$, measurements comprise 25 sinusoidal signals at various frequencies, three measurements per decade, and the measurements are log-spaced in the frequency range from 1 mHz to 45 kHz. Current was driven at the current electrodes A and B (Fig. 3) by a potential difference of 5 V. Both Cu/CuSO₄

(home-made) and Pb/PbCl₂ (Petiau electrodes, manufactured by Geonosis in France) had been tested. The Cu/CuSO₄ electrodes have a 12 mm diameter porous ceramic with a pore mean diameter of 2 μm and a hydraulic conductivity of $2.2 \times 10^{-9} \text{ m s}^{-1}$. The electrodes are made by a 10 cm length flexible plastic tube filled with CuSO₄ solution in which a 10 cm length copper wire (diameter of 1 mm) is inserted.

All the measurements performed with the NW oil have been done with both types of electrodes to compare the results. We found that (1) the experimental data were very similar, especially in low-frequency range from 10 mHz to 500 Hz and (2) accurate measurements could not always be achieved in the very low-frequency range (1 to 10 mHz) with the Cu/CuSO₄ electrodes because of leakages of the copper sulfate solution in the tank generating sometimes instable readings. Therefore only the Petiau electrodes were used in the entire frequency range from 1 mHz to 45 kHz and are shown later. We used a square array of electrodes with AB = MN = AM = BN = 7 cm because it was the easiest electrode array to use with our tank geometry. However the response should be independent of the selection of the electrode array as the sand in the sandbox is homogeneously distributed.

For all the experiments, the preparation of adequate quantities of sand, oil and water was performed about 30 min before the beginning of the measurements. We mixed the different components in the box shown in Fig. 3. We first mixed oil with water and then the oil/water mixture was mixed together with the sand. The same amount of sand was used for all the experiments. At saturation with water, the porosity was estimated from the volume of the box, the mass of the sand, and the density of silica (2650 kg m⁻³). The measured porosity is 0.40 ± 0.02 . The electrodes were inserted in the oil/sand/water mixture at a precise depth of $2 \text{ cm} \pm 1 \text{ mm}$ (Fig. 3). The duration of a complete cycle of measurements was 90 min, most of the time required to do the measurements being used to perform the measurements at lowest frequencies. Except when shown on the figures, the estimated phase uncertainty was 0.1 mrad based on the tests reported in Zimmermann *et al.* (2008).

A typical plot of the phase versus the frequency is shown in Fig. 4. A clear relaxation can be observed at low frequency and this relaxation is usually considered to be due to the polarization of the electrical double layer coating the sand grains (see Leroy *et al.* 2008 for a complete modelling of this contribution in sands). At high frequencies (>100 Hz), the phase increases because of the Maxwell–Wagner polarization as discussed extensively by Leroy *et al.* (2008). In this paper, we are however interested in the low-frequency behaviour and we will plot only the low-frequency range of the investigated frequency range.

4 EXPERIMENTAL RESULTS AND INTERPRETATION

All spectral induced polarization phase curves show a peak at low frequencies (in the 0.001–0.1 Hz range), consistent with results presented recently by Cassiani *et al.* (2009) who used a NW oil. The values of the phase angles and the resistivity at the peak of the relaxation are reported in Table 4. Measurements were done at five different saturations: $s_w = 1$ (the pore space is fully saturated with water), $s_w = 0.80$, $s_w = 0.60$, $s_w = 0.40$ and $s_w = 0.20$. In the case of the pore space fully saturated by oil, it was impossible to inject current in the sand/oil mixture because of the high resistivity of the oil (typically 10^9 ohm m).

Both the magnitude of the resistivity and the absolute value of the phase increases when the water saturation decreases. The resistivity

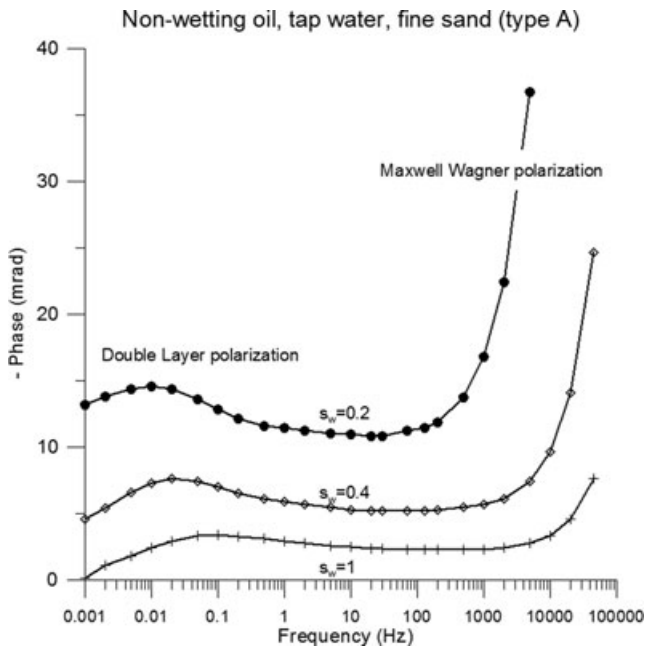


Figure 4. Full spectra of the phase shift between the current and the voltage. The low (ordinary) frequency polarization is usually considered to be due to electrical polarization phenomena with possibly a contribution from membrane polarization (see Vinegar & Waxman 1984) whereas at higher frequencies, the response is controlled by the Maxwell–Wagner polarization. This Maxwell–Wagner contribution to the overall polarization is not considered in this study.

Table 4. Values of the phase and the modulus of the resistivity at the peak of the relaxation for a sand (Type A) saturated by the NW oil.

Water saturation s_w (-)	Phase (mrad)	Resistivity (ohm m)
1.0	-3.4	279.1
0.8	-4.3	449.6
0.6	-5.7	853.7
0.4	-7.6	1740.0
0.2	-14.5	9149.2

increased from 300 ohm m for $s_w = 1$ to 10 000 ohm m for $s_w = 0.2$. The absolute value of the phase increased from 3.4 mrad for $s_w = 1$ to 14.5 mrad for $s_w = 0.2$ (Fig. 5). We also observed a shift in the frequency of the peak from 100 mHz at $s_w = 1$ to 10 mHz at $s_w = 0.2$.

To check the influence of the salinity of the pore water, we did four experiments at two water saturations ($s_w = 0.4$ and 0.6) with two different types of pore waters (Fig. 6). We used tap water (conductivity varying from $1.20 \times 10^{-2} \text{ S m}^{-1}$ and $1.70 \times 10^{-2} \text{ S m}^{-1}$ at $21 \pm 1^\circ\text{C}$) and demineralized water. We observed a slight shift of the peak of the polarization with the change in the ionic strength (from 20 mHz with tap water to 50 mHz with demineralized water). This is consistent with the fact that the peak of the phase is not expected to be very sensitive to the conductivity of the pore water, see eq. (14). The most dramatic change concerns the amplitude of the phase, which is much stronger for demineralized water ($\varphi = 11.3 \text{ mrad}$ for $s_w = 0.6$ and $\varphi = 12.3 \text{ mrad}$ for $s_w = 0.4$) than for tap water ($\varphi = 5.7 \text{ mrad}$ for $s_w = 0.6$ and $\varphi = 7.6 \text{ mrad}$ for $s_w = 0.4$). This is consistent with the model developed by Revil & Florsch (2010) and explained by the salinity dependence of the specific surface conductivity Σ^S .

To also check the influence of the grain size, we performed experiments at two distinct water saturations ($s_w = 0.4$ and 0.6) for the two types of sands: Types A ($200 \mu\text{m}$) and B ($500 \mu\text{m}$). The results are shown in Fig. 7. The resistivities did not show a strong dependence with the grain size at $s_w = 0.6$ and at $s_w = 0.4$. The effect of grain size is associated with surface conductivity in the electrical double layer surrounding the grains (Fig. 1). The conductivity is given by

$$\sigma = \frac{s_w^n}{F} \left[\sigma_w + (F - 1) \frac{4\Sigma^S}{s_w D_{50}} \right]. \quad (29)$$

We use the following values for the model parameters: $D_{50} = 200 \mu\text{m}$ (Type A), $D_{50} = 500 \mu\text{m}$ (Type B), $\sigma_w = (1.4 \pm 0.2) \times 10^{-2} \text{ S m}^{-1}$ (tap water), $F = 3.9$, $\Sigma^S = 2 \times 10^{-9} \text{ S}$ (see later), and $n = 2.14$ (see later). For $s_w = 0.6$, we find $\rho(\text{sand A}) = 820 \text{ ohm m}$ (measured $\sim 850 \text{ ohm m}$) and $\rho(\text{sand B}) = 827 \text{ ohm m}$ (measured $\sim 850 \text{ ohm m}$). For $s_w = 0.4$, we find $\rho(\text{sand A}) = 1939 \text{ ohm m}$ (measured $\sim 1600 \text{ ohm m}$) and $\rho(\text{sand B}) = 1963 \text{ ohm m}$ (measured $\sim 1500 \text{ ohm m}$). So surface conductivity can be neglected

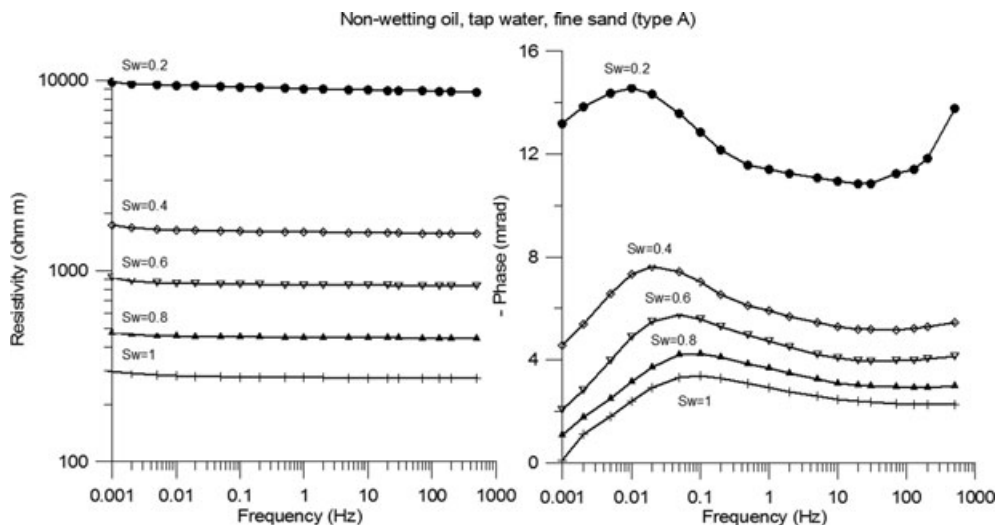


Figure 5. Modulus and phase of the complex resistivity for a NW oil for different values of the relative water saturations in the range 1.0 to 0.2 (the case corresponding to the fully oil saturated sand could not be measured). Sand: Type A (fine sand).

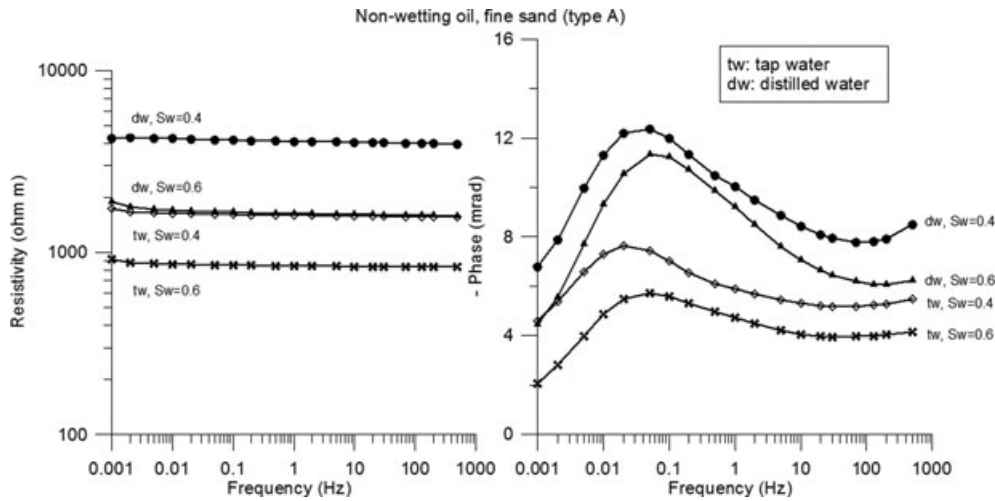


Figure 6. Modulus and phase of the complex resistivity for a NW oil for two different values of the water saturations $s_w = 0.6$ and $s_w = 0.4$ for two values of the conductivity of the pore water. Sand: Type A (fine sand). Note that smaller is the conductivity of the pore water, higher the value of the phase angle. The error bars are explicitly shown except when they are on the order of the size of the symbols or smaller.

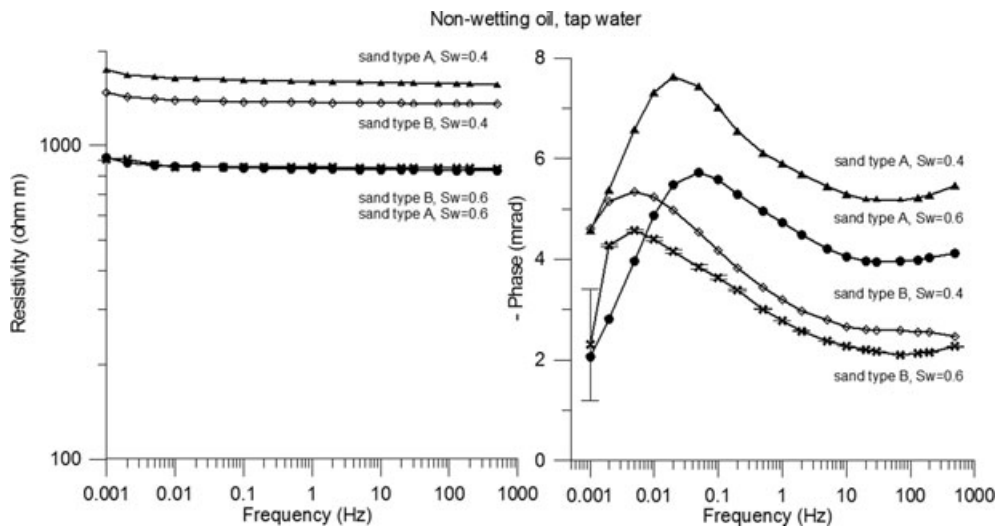


Figure 7. Modulus and phase of the complex resistivity for a NW oil for two different values of the water saturations $s_w = 0.6$ and $s_w = 0.4$ and for two values of the mean grain size. Sand: Type A (fine sand) and Type B (coarse sand). Note that the finest sand corresponds to the highest value of the absolute value of the phase angle and the highest specific surface area and surface conductivity. The error bars are explicitly shown except when they are on the order of the size of the symbols or smaller.

in the in-phase conductivity. It represents ~ 1 per cent of the in phase conductivity response for sands A and B for the pore waters used in this study. Therefore the in phase conductivity is unable to distinguish the two types of sands.

With the phase (or the quadrature conductivity), it is easier to distinguish the two types of sands because there a strong shift in the maximum of the phase maxima can be observed (Fig. 7). Type A ($200 \mu\text{m}$) sand has a peak frequency occurring at higher frequencies than Type B sand ($500 \mu\text{m}$). The measured peak of the (ordinary) frequency f_0 is in the range 60–100 mHz for type A at saturation in water (Figs 5 and 8) and 2 to 6 mHz for sand B (see Fig. 5). These results are consistent with the fact that the peak of the frequency depends on the square of the grain size: the larger the grain size, the smaller the frequency peak. According to our model, the relaxation frequency (in Hz) is defined as $f_0 = \omega_0/2\pi = 1/\tau_0 = 4D_S^i/(\pi\alpha D_{S0}^2)$. Taking $D_S^i = 2.5 \times 10^{-9} \text{ m}^2 \text{ s}^{-1}$ (Leroy *et al.* 2008) and a tortuosity $\alpha = 1.56$ (given as the

product of the formation factor by the connected porosity), the relaxation frequency is 51 mHz for Type A and 8 mHz for Type B. Therefore there is a fair agreement between the theory and the observations. Type A is also characterized by phases that are higher than Type B. This is consistent with the fact that a pack of small grains has a surface area higher than a pack of coarser grains (see discussion in Section 2).

In Fig. 8, we mixed in equal volume Sand A (fine) and Sand B (coarse) and we measured the complex conductivity of the mixture using the same procedure as before. The spectrum of the phase is compared with the spectra obtained with Sand A and Sand B at full water saturation (see Fig. 8). At 100 Hz the phase is found to be exactly in between the phase of Sand A and Sand B. The frequency peak of the mixture (~ 30 – 50 Hz) is observed to be closer to the frequency peak of Sand A (60–100 mHz) than to the frequency peak of sand B (~ 1 – 6 mHz). These results are also qualitatively in agreement with our model as the characteristic grain size of a

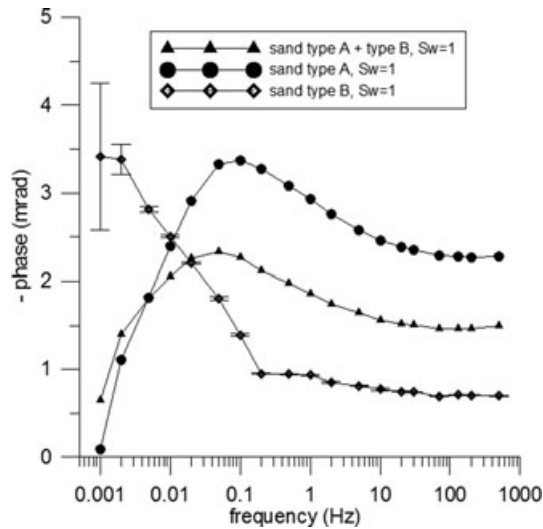


Figure 8. Phase of the complex resistivity for a 1:1 mixture (in volume) of sand A (fine sand) and sand B (coarse sand) compared with the phase spectra for Sand A and Sand B at full water saturation. The error bars are explicitly shown except when they are on the order of the size of the symbols or smaller.

multimodal distribution is given by Revil & Florsch 2010,

$$\frac{1}{E_h} = \left(\int_0^{+\infty} f(D) d \ln D \right)^{-1}. \quad (30)$$

If we consider a mixture of two very narrow grain size distributions (described by two delta functions), we can write (Revil & Florsch 2010):

$$\frac{1}{E_h} = \frac{1}{f_f/D_f + f_c/D_c}, \quad (31)$$

where f_f is the volumetric fraction of fine grains of diameter D_f and f_c is the volumetric fraction of coarse grains of diameter D_c . In our case $f_f = f_c = 1/2$, $D_f = 200 \mu\text{m}$, $D_c = 500 \mu\text{m}$. Using eq. (31), this yields $1/E_h = 286 \mu\text{m}$. Replacing D_{50} in the expression of the peak frequency by $1/E_h$, the relaxation frequency (in Hz) is given as $f_0 = 4D_{50}^2 E_h^2 / (\pi \alpha)$. This yields a relaxation frequency of 25 mHz in fair agreement with the observed frequency peak of the mixture (~ 30 – 50 mHz).

We come back now to the in phase conductivity. The small dependence of the electrical conductivity with the grain size implies that surface conductivity can be neglected. Therefore, according to eq. (4), we can write

$$\sigma = \frac{1}{F} s_w^n \sigma_w. \quad (32)$$

From Fig. 9(a), the formation factor can be determined experimentally as 275 ohm m divided by the resistivity of the pore water. The conductivity of the pore water is $\sigma_w = (1.4 \pm 0.2) \times 10^{-2} \text{ S m}^{-1}$, so the formation factor is 3.9. This is consistent with a porosity of 0.40 and a cementation exponent of 1.5. The experimental data obey also the second Archie's law with a saturation exponent n equal to 2.14 (see Fig. 9). Vinegar & Waxman (1984, their table 10) reported a mean value of the exponent term equal to 2.06 for sandstones. We use the following power-law relationship to fit the values of the phase (at the frequency of the peak of the low-frequency relaxation) with the saturation:

$$\varphi_0 = a s_w^{-b}. \quad (33)$$

We find $a = -3.5 \pm 0.5$ mrad and the exponent term is $b = 0.89 \pm 0.10$. In the case of the exponent, the theoretical value obtained in Section 2 (equation 22) is $b = 1$. According to our model, the constant a is given by

$$a = -\frac{2\Sigma^S(F-1)}{\sigma_w D_{50}} \exp\left(\frac{1}{2}\hat{\sigma}^2\right). \quad (34)$$

The formation factor is equal to $F = 3.9$ (see earlier). The conductivity of the pore water is $\sigma_w = (1.4 \pm 0.2) \times 10^{-2} \text{ S m}^{-1}$. The mean diameter of the grains is $D_{50} = 200 \pm 10 \mu\text{m}$ (see Table 1). With the values of the standard deviation reported in Table 1 (corresponding to a very narrow grain size distribution), the exponential term is very close to one (1.04 for sand A and closer to 1 for sand B). The specific surface conductivity Σ^S found by Bolève *et al.* (2007) is equal to $4 \times 10^{-9} \text{ S}$ at 25°C . They used sodium chloride solutions. In this case, the solution is dominated by the bivalent cation Ca^{2+} in the pore water (see Table 2). The presence of bivalent counterions decreases by a factor two the inner potential of the diffuse layer (Lorne *et al.* 1999, their fig 18) and therefore the specific surface conductance. Therefore, we consider $\Sigma^S = 2 \times 10^{-9} \text{ S}$ in eq. (31) to determine the value of the coefficient a . This yields $a = -4.1 \pm 0.7$ mrad. This value is consistent with the value determined from the fit of the experimental data $a = -3.5$ mrad (see earlier). So both coefficients a and b can be predicted by the model.

Another way to represent the data is to plot the quadrature conductivity as a function of the frequency or the water saturation. Some authors prefer this representation of the data as the quadrature conductivity is independent of the in-phase conductivity whereas the phase angle depends both on the in-phase and quadrature conductivities. However one can argue that the in-phase and quadrature conductivities are not independent either as they depends on the same parameters (formation factor, specific surface conductance). The results are shown in Fig. 10. The quadrature conductivity at the relaxation frequency (denoted with a subscript m) increases with the water saturation.

$$\sigma_0'' = c s_w^p, \quad (35)$$

And according to our model, we have

$$c = -\frac{1}{D_{50}} \left(\frac{F-1}{F} \right) \Sigma^S \exp\left(\frac{1}{2}\hat{\sigma}^2\right), \quad (36)$$

and $p = n - 1$. Using n equal to 2.14 (see earlier), the theoretical value predicted by our model is $p = 1.14$. Using $F = 3.9$ (see earlier), $D_{50} = 200 \mu\text{m}$, a narrow grain size distribution such as the exponential term is equal to one, and $\Sigma^S = 2 \times 10^{-9} \text{ S}$, the theoretical value of c is equal to $1.6 \times 10^{-5} \text{ S m}^{-1}$. These values can be compared to the experimental values $p = 1.26$ (Fig. 11) and $c = 1.3 \times 10^{-5} \text{ S m}^{-1}$ (Fig. 10). There is again a good agreement between the theory and the experimental data.

Fig. 10 shows the dependence of the normalized quadrature conductivity versus water saturation for the sand filled with the NW oil and water and for two sandstones investigated by Vinegar & Waxman (1984). The normalization is done with respect to the value of the quadrature conductivity at saturation of the water phase. Our results are consistent with those of Vinegar & Waxman (1984). According to the model developed earlier and the model of Vinegar & Waxman (1984), the exponent of this relationship is $p = n - 1$. As $n = 2.14$ for our sample and the mean of n is equal to 2.06 for the samples investigated by Vinegar & Waxman (1984, their table 10), we expect $p = 1.14$ in our case and $p = 1.06$ in the case of the data reported by Vinegar & Waxman (1984). We observe an exponent that is equal to 1.26 for our data. Vinegar & Waxman (1984,

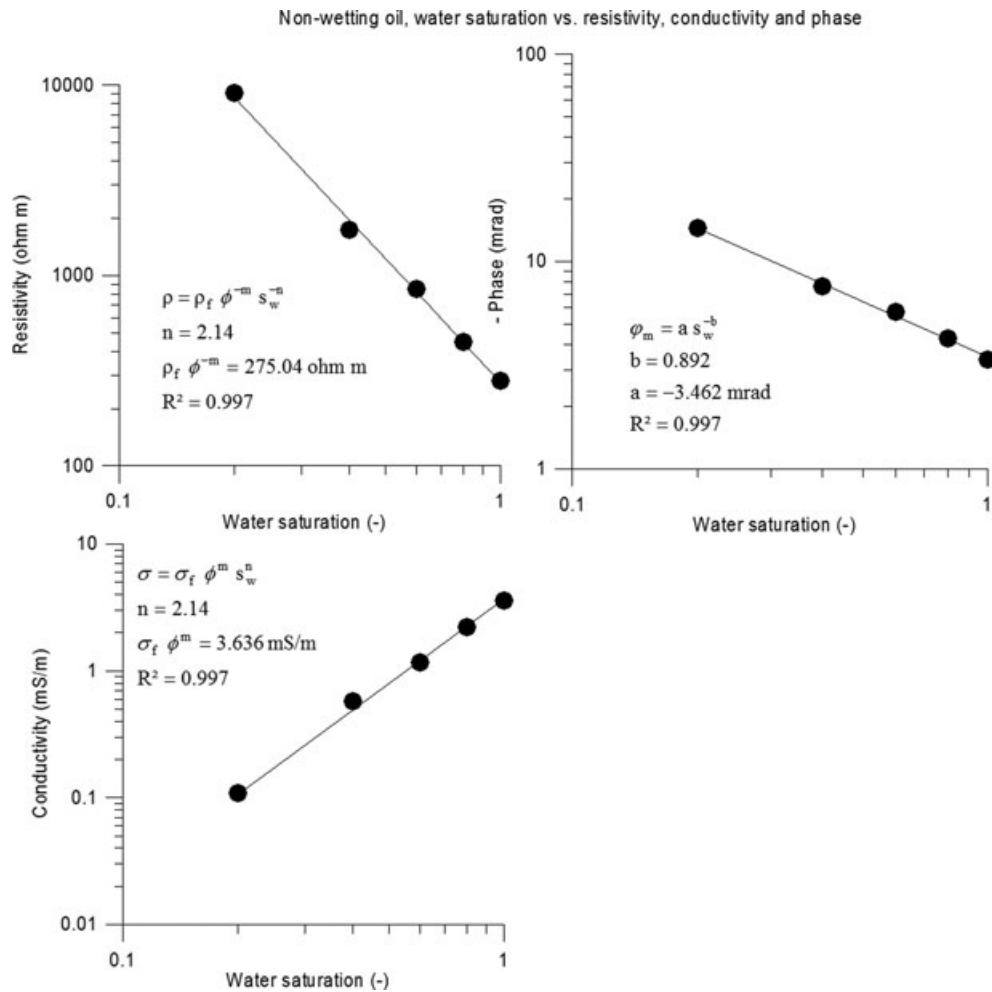


Figure 9. Modulus and peak value of the phase of the complex resistivity/conductivity for a NW oil as a function of the saturation of the water phase. Type A (fine sand). The fit of the linear trend between the resistivity and the saturation provides a value for the second Archie's exponent n when surface conductivity can be neglected in the in phase conductivity.

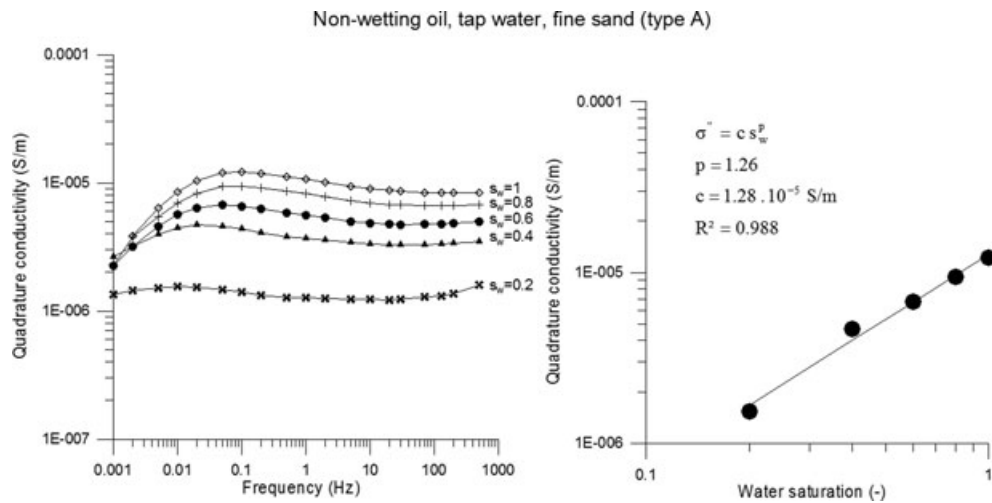


Figure 10. Left-hand side: Quadrature or imaginary component of the complex conductivity versus the ordinary frequency f . Right-hand side: Quadrature or imaginary component of the complex conductivity versus the water saturation at the frequency corresponding to the low-frequency peak of the phase.

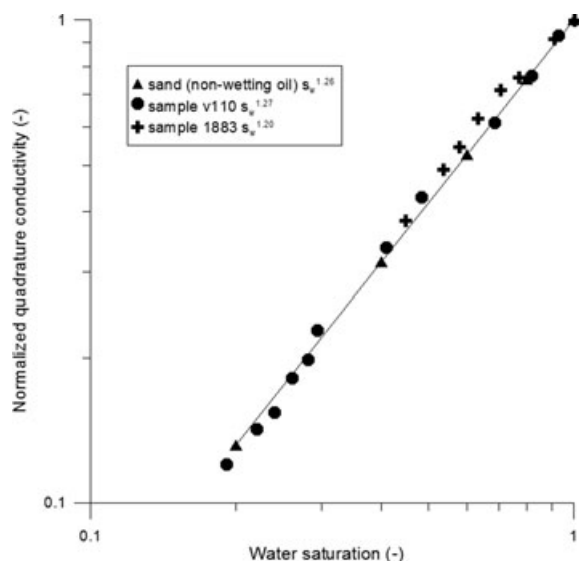


Figure 11. Quadrature (imaginary) conductivity versus water saturation. Comparison between our results for the sand filled with the NW oil and the two sandstone samples investigated by Vinegar & Waxman (1984). The values reported on the figure represent the values of the exponent p (the line represents the linear trend with $p = 1.26$).

$p = 1.282$) found $p = 1.11 \pm 0.17$. Therefore, the agreement between our model and the experimental data is fairly good.

5 CONCLUDING STATEMENTS

We have performed spectral induced polarization measurements with fresh oil-bearing sands investigating the influence of different parameters including (1) the oil saturation, (2) the conductivity of the pore water, and (3) the mean grain diameter of the sand. Our goal was to extend and to further test the spectral induced polarization model developed recently by Revil & Florsch (2010). This model is based on the polarization of the Stern layer at the sand/water interface and the polarization length scale is the size of the grains because of the discontinuity of the Stern layer between grains. For a NW oil, the absolute value of the phase increases with the oil saturation and decreases with the salinity. An increase of the mean grain diameter shifts the peak frequency at lower frequencies and decreases the value of the phase in a predictable way. All these results obtained with the NW oil can be reproduced with the extension of the Revil & Florsch model except the broadness of the distribution of relaxation times that remains unexplained. The explanation may be found in the membrane polarization that has not been incorporated yet in our model or in mutual polarization effects between the grains that are not captured by the convolution product (David Lesmes, personal communication, 2010). The application of the present model to *in situ* measurements will require the determination of the temperature dependence of the in-phase and quadrature conductivities and the experimental results and temperature dependence of surface conductivity shown by Vinegar & Waxman (1984) could be used for this purpose. The change of chemistry and biochemistry of an oil undergoing biodegradation in the subsurface would be probably reflected by a change in the time-lapse induced polarization signature and wettability of the oil. This is something worth to investigate in future works.

ACKNOWLEDGMENTS

We thank Office of Science (BER), US Department of Energy, Grant No. DE-FG02-08ER646559 for financial support, Agency of Environment and Energy Management (ADEME) and Region Aquitaine in France (FEDER Project). We thank G. Olhoeft and A. Binley for fruitful discussions and K. Schmidt for her help with the experiments. We thank two anonymous referees for their very constructive comments and the Editor Jörg Renner. Although this work was reviewed by EPA and approved for presentation, it may not necessarily reflect official Agency policy. Mention of trade names or commercial products does not constitute endorsement or recommendation by EPA for use.

REFERENCES

- Archie, G.E., 1942. The electrical resistivity log as an aid in determining some reservoir characteristics, *Trans. Am. Inst. Mining Metall. Eng.*, **146**, 54–62.
- Binley A., Slater, L., Fukes, M. & Cassiani, G., 2005. The relationship between frequency dependent electrical conductivity and hydraulic properties of saturated and unsaturated sandstone, *Water Resour. Res.*, **41**(13), W12417.
- Binley A., Kruschwitz, S., Lesmes, D. & Kettridge, N., 2010. Exploiting the temperature effects on low frequency electrical spectra of sandstone: determination of effective diffusion path lengths, *Geophysics*, in press.
- Bolève, A., Crespy, A., Revil, A., Janod F. & Mattiuzzo J. L., 2007. Streaming potentials of granular media: influence of the Dukhin and Reynolds numbers, *J. geophys. Res.*, **112**, B08204, doi:10.1029/2006JB004673.
- Börner, F., Gruhne, M. & Schön, J., 1993. Contamination indications derived from electrical properties in the low frequency range, *Geophys. Prospect.*, **41**, 83–98.
- Cassiani, G., Kemna, A. & Villa, A., 2009. Spectral induced polarization for the characterization of free-phase hydrocarbon contamination of sediments, *Near Surf. Geophys.*, **7**(5–6), 547–562.
- City of Golden, 2009. *Water Quality Report*, 8pp, City of Golden Public Works Department, Golden, CO.
- Ghorbani, A., Cosenza, Ph., Ruy, S., Doussan, C. & Florsch, N., 2008. Noninvasive monitoring of water infiltration in a clay loamy soil using Spectral Induced Polarization, *Water Resour. Res.*, **44**, W08402, doi:10.1029/2007WR006114.
- Jougnot D., Ghorbani, A., Revil, A., Leroy, P. & Cosenza, P., 2010. Spectral induced polarization of partially saturated clay-rocks: a mechanistic approach, *Geophys. J. Int.*, **180**(1), 210–224, doi:10.1111/j.1365-246X.2009.04426.x.
- Leroy, P. & Revil, A., 2009. Spectral induced polarization of clays and clay-rocks, *J. geophys. Res.*, **114**, B10202, doi:10.1029/2008JB006114.
- Leroy P., Revil, A., Kemna, A., Cosenza, P. & Gorbani, A., 2008. Spectral induced polarization of water-saturated packs of glass beads, *J. Colloid Interface Sci.*, **321**(1), 103–117.
- Lesmes, D.P. & Morgan, F.D., 2001. Dielectric spectroscopy of sedimentary rocks, *J. geophys. Res.*, **106**(B7), 13 329–13 346.
- Li, Y., Yue, Q. & Gao, B., 2010. Adsorption kinetics and desorption of Cu(II) and Zn(II) from aqueous solution onto humic acid, *J. Hazardous Mater.*, **178**, 455–461.
- Linde, N., Jougnot, D., Revil, A., Matthäi, S.K., Arora, T., Renard, D. & Doussan C., 2007. Streaming current generation in two-phase flow conditions, *Geophys. Res. Lett.*, **34**(3), L03306, doi:10.1029/2006GL028878.
- Lorne, B., Perrier, F. & Avouac, J.P., 1999. Streaming potential measurements 1. Properties of the electrical double layer from crushed rock samples, *J. geophys. Res.*, **104**(B8), 17 857–17 877.
- Marshall, D.J. & Madden T.R., 1959. Induced polarization, a study of its causes, *Geophysics*, **24**, 790–816.
- Olhoeft, G.R., 1985. Low-frequency electrical properties, *Geophysics*, **50**, 2492–2503.
- Olhoeft, G.R., 1986. Direct detection of hydrocarbon and organic chemicals with ground-penetrating radar and complex resistivity: petroleum,

- hydrocarbons and organic chemicals in ground water-prevention, detection, and restoration, in *Proceedings of the NWWA/API Conference on Petroleum Hydrocarbons and Organic Chemicals in Ground Water – Prevention, Detection and Restoration*, pp. 284–305, eds Graves B.J. *et al.*, Nat. Water Well Assoc., Dublin, OH.
- Revil A., 1999. Ionic diffusivity, electrical conductivity, membrane and thermoelectric potentials in colloids and granular porous media: a unified model, *J. Colloid Interf. Sci.*, **212**, 503–522.
- Revil, A. & Florsch, N., 2010. Determination of permeability from spectral induced polarization in granular media, *J. geophys. Int.*, **181**, 1480–1498, doi:10.1111/j.1365-246X.2010.04573.x.
- Revil, A., Schwaeger, H., Cathles, L.M. & Manhardt P., 1999. Streaming potential in porous media. Part 2. Theory and application to geothermal systems, *J. geophys. Res.*, **104**(B9), 20 033–20 048.
- Revil, A., Leroy, P. & Titov, K., 2005. Characterization of transport properties of argillaceous sediments. Application to the Callovo-Oxfordian Argillite, *J. geophys. Res.*, **110**, B06202, doi:10.1029/2004JB003442.
- Revil A., Linde, N., Cerepi, A., Jougnot, D., Matthäi, S. & Finsterle S., 2007. Electrokinetic coupling in unsaturated porous media, *J. Colloid Interf. Sci.*, **313**(1), 315–327, doi:10.1016/j.jcis.2007.03.037.
- Sakaki, T., 2009. Physical, hydraulic, and thermal properties of silica sands for laboratory experiments, in *Proceedings of the Internal Report, Center for Experimental Study of Subsurface Environmental Processes (CESEP)*, Colorado School of Mines, Golden, Colorado.
- Sakaki, T. & Illangasekare, T.H., 2007. Comparison of height-averaged and point-measured capillary pressure–saturation relations for sands using a modified Tempe cell, *Water Resour. Res.*, **43**, W12502, doi:10.1029/2006WR005814.
- Schwarz, G., 1962. A theory of the low-frequency dielectric dispersion of colloidal particles in electrolyte solution, *J. Phys. Chem.*, **66**, 2636–2642.
- Sen, P.N., Scala, C. & Cohen, M.H., 1981. A self-similar model for sedimentary rocks with application to the dielectric constant of fused glass beads, *Geophysics*, **46**(5), 781–795.
- Slater, L. & Lesmes, D., 2002a. IP interpretation in environmental investigations, *Geophysics*, **67**(1), 77–88.
- Slater, L. & Lesmes, D., 2002b. Electrical-hydraulic relationships observed for unconsolidated sediments, *Water Resour. Res.*, **38**(10), 1213.
- Sturrock, J.T., 1999. Predictions of hydraulic conductivity using spectral induced polarizations, *Ms dissertation*, Boston College.
- Ulrich, C. & Slater, L.D., 2004. Induced polarization measurements on unsaturated, unconsolidated sands, *Geophysics*, **69**(3), 762–771.
- Vanhala, H., 1997. Mapping oil-contaminated sand and till with the spectral induced polarization (SIP) method, *Geophys. Prospect.*, **45**, 303–326.
- Vanhala, H., Soininen, H. & Kukkonen, I., 1992. Detecting organic chemical contaminants by spectral-induced polarization method in glacial till environment, *Geophysics*, **57**, 1014–1017.
- Vinegar, H.J. & Waxman, M.H. 1982. Method and apparatus for determining shaliness and oil saturations in earth formations using induced polarization in the frequency domain, U.S. Patent no. 4, 359,687.
- Vinegar, H.J. & Waxman M.H., 1984. Induced polarization of shaly sands, *Geophysics*, **49**, 1267–1287.
- Volkov A.G., Deamer, D.W., Tanelian, D.L. & Markin V.S., 1996. Electrical double layer at the oil/water interface, *Progress in Surface Science*, **53**(1), 1–134.
- Waxman, M.H. & Smits, L.J.M., 1968. Electrical conductivities in oil bearing shaly sands, *Soc. Pet. Eng. J.*, **8**, 107–122.
- Zimmermann, E., Kemna, A., Berwix, J., Glaas, W., Münch, H.M. & Huisman, J.A., 2008. A high-accuracy impedance spectrometer for measuring sediments with low polarizability, *Meas. Sci. Technol.*, **19**, doi:10.1088/0957-0233/19/10/105603.

APPENDIX A: COMPARISON WITH THE VINEGAR AND WAXMAN MODEL

The Vinegar & Waxman (1982, 1984) model was developed to determine the phase and the resistivity of oil-bearing sandstones partially saturated with NW oils. In this model, the distribution of

the relaxation times is considered to be very broad but it is not explicitly accounted for. Therefore, over a broad frequency range, the in-phase and quadrature conductivities are frequency independent. At the opposite, in our model the distribution of the relaxation times is explicitly taken into account through a convolution with the probability distribution of the inverse of the grain diameters. We show later that our model is, however, consistent with the equations developed by Vinegar & Waxman (1982, 1984) with the exception that our model accounts for the frequency dependence of the in-phase and quadrature conductivities with frequency.

From eq. (4), the low-frequency electrical conductivity is given by

$$\sigma = \frac{s_w^n}{F} [\sigma_w + s_w^{-1} (\beta_{(+)} \bar{Q}_V + (F - 1) \sigma_S)]. \quad (A1)$$

Using a first-order Taylor expansion of Archie's law for a pack of spherical grains characterized by a value of the cementation exponent equal to 1.5 (from the differential effective medium theory applied to purely spherical grains, see Sen *et al.* 1981), the term $(F - 1)$ at high porosities is approximated by

$$F - 1 = \frac{3}{2} \left(\frac{1 - \phi}{\phi} \right) + \dots \quad (A2)$$

The in-phase surface conductivity associated with the Stern layer is given by

$$\sigma'_S = \frac{2}{3} \left(\frac{\phi}{1 - \phi} \right) \beta_{(+)} f Q_V, \quad (A3)$$

where f is the fraction of surface conductivity due to the Stern layer ($0 \leq f \leq 1$), $(1 - f)$ is the fraction of surface conductivity due to the diffuse layer, and the factor $2\phi/[3(1 - \phi)]$ represents a conversion factor to convert a charge per unit surface of the mineral to a charge per unit pore volume. In eq. (A3), Q_V represents the total charge per unit volume including the Stern and the diffuse layer contributions. The charge density Q_V can be determined from the Cation Exchange Capacity (CEC, expressed in C kg⁻³) of the rock (Waxman & Smits 1968):

$$Q_V = \rho_S \left(\frac{1 - \phi}{\phi} \right) \text{CEC}, \quad (A4)$$

where ρ_S is the mass density of the solid phase (in kg m⁻³) and ϕ is the connected porosity. In addition, we have $\bar{Q}_V = (1 - f) Q_V$. Combining eqs (A1) to (A3), the in-phase conductivity is given by

$$\sigma' = \frac{1}{F} s_w^n \left(\sigma_w + \frac{\beta_{(+)} Q_V}{s_w} \right). \quad (A5)$$

Eq. (A4) corresponds to the Waxman & Smits (1968) model. The quadrature conductivity is assumed related to the quadrature conductivity of the surface conductivity by

$$\sigma'' = \frac{(F - 1) s_w^{n-1}}{F} \sigma_S''. \quad (A6)$$

At high porosity, inserting eq. (A2) into eq. (A6), we have

$$\sigma'' \approx \frac{3(1 - \phi) s_w^{n-1}}{2 \phi F} \sigma_S''. \quad (A7)$$

Assuming that,

$$\sigma_S'' = -\frac{2}{3} \left(\frac{\phi}{1 - \phi} \right) \beta_{(+)} f Q_V, \quad (A8)$$

and inserting eq. (A8) into eq. (A7), the quadrature conductivity is given by

$$\sigma'' = -\frac{s_w^{n-1}}{F} \beta_{(+)} f Q_V. \quad (A9)$$

This can be compared with the quadrature conductivity model of Vinegar & Waxman (1984, their eq. 36),

$$\sigma'' = -\frac{s_w^{n-1}}{F} \lambda_a \bar{Q}_V. \quad (\text{A10})$$

A comparison between eqs (A9) and (A10) implies $\lambda_a = \beta_{(+)} f$. Taking $f = 0.84$ (see Revil & Florsch 2010), we obtain $\lambda_a = 4.3 \times 10^{-8} \text{ m}^2 \text{ s}^{-1} \text{ V}^{-1}$ using the mobility of sodium in water ($5.19 \times 10^{-8} \text{ m}^2 \text{ s}^{-1} \text{ V}^{-1}$ at 25°C) and $\lambda_a = 4 \times 10^{-9} \text{ m}^2 \text{ s}^{-1} \text{ V}^{-1}$ using the value of the mobility of sodium along the mineral surface suggested by Revil (1999, his Table 1) ($0.51 \times 10^{-8} \text{ m}^2 \text{ s}^{-1} \text{ V}^{-1}$ at 25°C). The value given by Vinegar & Waxman (1982, 1984, their table 5) is equal to $\lambda_a = 4 \pm 2 \times 10^{-9} \text{ m}^2 \text{ s}^{-1} \text{ V}^{-1}$. However it would be presumptuous to conclude too quickly that the mobility of the counterions in the Stern layer is necessarily ten times lower than in the bulk pore water. Vinegar & Waxman (1982, 1984) indicated that in addition to the polarization of the mineral surface, there is an additional polarization mechanism called the membrane polarization effect, which is not included in our model. In addition, our model would predict a distribution of relaxation times that is narrower than observed in the experiment reported in the main text. This may point out that another hidden mechanism, like membrane polarization, is at play.

APPENDIX B: EXTENSION OF THE REVIL AND FLORSCH MODEL

For a water-saturated sand, the model developed by Revil & Florsch (2010) can be recasted as

$$\sigma(\omega) = \frac{1}{F} [\sigma_w + \beta_{(+)} \bar{Q}_V + (F - 1) \sigma_S(\omega)]. \quad (\text{B1})$$

The first term in brackets corresponds to the frequency-independent conductivity of the brine, the second term corresponds to the frequency-independent surface conductivity associated with the diffuse layer, and the third term corresponds to the frequency dependent surface conductivity term associated with the Stern layer. Extending this model for partial saturations requires making this model compatible with some well-known relationships. One of them is the second Archie's law when surface conductivity can be neglected. This law states that the inverse of the formation factor should be replaced by $(1/F)s_w^n$ at partial saturation s_w . When surface conductivity can be neglected, this yields,

$$\sigma = \frac{1}{F} s_w^n \sigma_w, \quad (\text{B2})$$

where n is the second Archie's exponent. In addition, we know from electrokinetic measurements that the excess of charge per unit volume scales as \bar{Q}_V/s_w for conditions of partial saturations (see Revil *et al.* 2007 and Linde *et al.* 2007). Assuming that the whole surface conductivity contribution follows the same dependence, we obtain the following equation at partial saturation,

$$\sigma(\omega) = \frac{s_w^n}{F} \left[\sigma_w + \beta_{(+)} \frac{\bar{Q}_V}{s_w} + (F - 1) \frac{\sigma_S(\omega)}{s_w} \right]. \quad (\text{B3})$$